NeuroImage 143 (2016) 141–151

Contents lists available at ScienceDirect

NeuroImage

journal homepage: www.elsevier.com/locate/neuroimage

Noise contributions to the fMRI signal: An overview

Thomas T. Liu [a,b,*]

[a] Center for Functional MRI, University of California San Diego, 9500 Gilman Drive MC 0677, La Jolla, CA 92093, United States
[b] Departments of Radiology, Psychiatry and Bioengineering, University of California San Diego, 9500 Gilman Drive, La Jolla, CA 92093, United States

ARTICLE INFO

Article history:
Received 24 June 2016
Accepted 3 September 2016
Available online 6 September 2016

Keywords:
FMRI
Noise sources
Physiological noise
Motion
General linear model

ABSTRACT

The ability to discriminate signal from noise plays a key role in the analysis and interpretation of functional magnetic resonance imaging (fMRI) measures of brain activity. Over the past two decades, a number of major sources of noise have been identified, including system-related instabilities, subject motion, and physiological fluctuations. This article reviews the characteristics of the various noise sources as well as the mechanisms through which they affect the fMRI signal. Approaches for distinguishing signal from noise and the associated challenges are also reviewed. These challenges reflect the fact that some noise sources, such as respiratory activity, are generated by the same underlying brain networks that give rise to functional signals that are of interest.

1. Introduction

In a functional magnetic resonance imaging (fMRI) experiment, a time series of images is acquired with a temporal resolution (ranging from several hundred milliseconds to several seconds) that depends on the experimental design and the parameters of the MRI acquisition. The acquisition is designed to reflect changes in the apparent transverse relaxation rate, an MRI parameter that is sensitive to the amount of deoxyhemoglobin in the blood and exhibits a complex dependence on cerebral blood flow, metabolism, and volume (Buxton et al., 2004). This dependence forms the basis for blood oxygenation level dependent (BOLD) fMRI. The acquired time series data contain contributions from BOLD-weighted signal changes related to brain activity. In addition, there are a variety of undesired noise components (both BOLD and non-BOLD weighted) whose magnitude is often comparable or even greater than the signal of interest.

Over the past two decades, efforts to characterize and mitigate the effects of noise in BOLD fMRI time series have played an integral role in the development of fMRI acquisition and analysis approaches (Murphy et al., 2013; Greve et al., 2013; Birn, 2012). Advances in methods to distinguish signal from noise have led to improvements in the ability to detect and estimate brain activity. In this paper, we will review the primary sources of noise in fMRI, with a focus on the noise components that appear in fMRI time series signals. In-depth treatments of the various noise sources are provided elsewhere in this special issue. In the analysis of fMRI studies, there are additional sources of noise, such as inter-scan, inter-subject, and inter-site variability (Greve et al., 2013), but these sources will not be considered here.

We will begin by reviewing a basic signal model for BOLD fMRI and considering the various ways in which noise affects the elements of the model. This will be followed by an examination of the mechanisms through which various processes, such as cardiac and respiratory activity, can act as noise sources. We will conclude with an overview of approaches for separating signal from noise in fMRI.

As we consider the sources of noise in the fMRI time series, we will find that the line between signal and noise is not always clear. Whether a component is considered to be signal or noise depends on our current perspective and understanding of the underlying physiology and biophysics. Indeed, over the course of the history of fMRI, there have been several instances when a component that was originally considered to be noise has become a signal of great interest.

2. Signal and noise components

In order to understand the role of noise in BOLD fMRI, it useful to start with a basic signal model of the form

$$S(t) = S_0(t)\cdot\exp\left(-R_2^*(t)\cdot\mathrm{TE}\right) + n(t) \quad (1)$$

where $S(t)$ denotes the signal acquired at time t, $R_2^*(t)$ is the apparent transverse relaxation rate, TE denotes the echo time, $S_0(t)$ denotes the magnetization at zero echo time $\mathrm{TE} = 0$, and $n(t)$

* Correspondance address: Center for Functional MRI, University of California San Diego, 9500 Gilman Drive MC 0677, La Jolla, CA 92093, United States.
E-mail address: ttliu@ucsd.edu

http://dx.doi.org/10.1016/j.neuroimage.2016.09.008
1053-8119/

represents additive background noise.

For most fMRI experiments, it is the relative change $\Delta S/S$ in the measured signal that is typically of interest. To derive a simplified expression for this quantity, we first approximate the absolute change in the measured signal as

$$\begin{aligned}\Delta S(t) &\approx \Delta S_0(t)\cdot\frac{\partial S}{\partial S_0}\bigg|_{t=0} + \Delta R_2^*(t)\cdot\frac{\partial S}{\partial R_2^*}\bigg|_{t=0} + \Delta n(t)\\ &= \Delta S_0(t)\cdot\exp\big(-R_2^*(0)\cdot\mathrm{TE}\big)\\ &\quad - \Delta R_2^*(t)\cdot S_0(0)\cdot\exp\big(-R_2^*(0)\cdot\mathrm{TE}\big)\cdot\mathrm{TE} + \Delta n(t)\\ &\approx S(0)\cdot\frac{\Delta S_0(t)}{S_0(0)} - S(0)\cdot\mathrm{TE}\cdot\Delta R_2^*(t) + \Delta n(t)\end{aligned} \tag{2}$$

Dividing the final expression by the initial signal value $S(0)$ yields an expression for the relative change

$$\frac{\Delta S(t)}{S(0)} \approx \frac{\Delta S_0(t)}{S_0(0)} - \mathrm{TE}\cdot\Delta R_2^*(t) + \frac{\Delta n(t)}{S(0)} \tag{3}$$

as the sum of three terms: (1) the relative change in the magnetization at zero echo time $\frac{\Delta S_0(t)}{S_0(0)}$, (2) a term $\mathrm{TE}\cdot\Delta R_2^*(t)$ proportional to the change in relaxation rate, and (3) the relative change in the background noise term $\frac{\Delta n(t)}{S(0)}$. We are typically most interested in the $\mathrm{TE}\cdot\Delta R_2^*(t)$ term, as it is the change in the relaxation rate $R_2^*(t)$ that most directly reflects functional changes in blood oxygenation, flow, and volume. This term is sometimes referred to as the BOLD-like component, whereas the magnetization term is referred to as the non-BOLD component. In the sections below, we examine the role of noise in each of the terms.

In discussions of signal and noise in fMRI, a commonly used metric to characterize the performance of an acquisition is the temporal signal-to-noise-ratio (tSNR) (Parrish et al., 2000; Triantafyllou et al., 2005). This is defined as

$$\begin{aligned}\mathrm{tSNR} &= \frac{\text{Mean signal Amplitude}}{\text{Standard Deviation of the Noise Over Time}}\\ &= \frac{S_{mean}}{\sqrt{\sigma_T^2 + \sigma_{NB}^2 + \sigma_B^2}}\end{aligned} \tag{4}$$

where σ_T^2, σ_{NB}^2, σ_B^2 represent the noise variances of the background, non-BOLD, and BOLD-like components, respectively. The tSNR level determines the ability of an acquisition to detect activity-related changes, with smaller percent BOLD changes requiring a larger tSNR value. For example, Parrish et al. (2000) reported that to detect a 0.5% signal change (in a time series of 112 images) with a probability of detection of 0.95 and a probability of false alarm of 0.05, a tSNR of 138 would be required. The required tSNR is inversely proportional to the signal change, so that a 1% change would require a tSNR of 69 at the same probabilities of detection and false alarm.

As noted by Krüger and Glover (2001), it useful to rewrite tSNR as follows

$$\begin{aligned}\mathrm{tSNR} &= \frac{S_{mean}}{\sqrt{\sigma_T^2 + \sigma_p^2}}\\ &= \frac{S_{mean}/\sigma_T}{\sqrt{1 + \sigma_p^2/\sigma_T^2}}\\ &= \frac{\mathrm{SNR}_0}{\sqrt{1 + \lambda^2\mathrm{SNR}_0^2}}\end{aligned} \tag{5}$$

where $\mathrm{SNR}_0 = S_{mean}/\sigma_T$ represents the image SNR, the term $\sigma_p^2 = \sigma_{NB}^2 + \sigma_B^2$ is the sum of the non-BOLD and BOLD-like noise variances, and λ is a scaling factor that relates this term to the mean signal amplitude, such that $\sigma_p = \lambda S_{mean}$. This last relation reflects the fact that both the non-BOLD and BOLD terms in Eq. (2) are proportional to the signal term $S(0)$. For small image SNR values where $\lambda^2\mathrm{SNR}_0^2 \ll 1$, tSNR scales linearly with SNR_0. Since $\mathrm{SNR}_0 = \sigma_p/(\lambda\sigma_T)$, this can also be viewed as the regime in which the signal independent noise term σ_T is much greater than the signal dependent term σ_p. For example, for high resolution scans in which the voxel volume is relatively small, the thermal noise contributions (described in the next section) will tend to dominate the signal-dependent physiological noise terms. As image SNR increases such that $\lambda^2\mathrm{SNR}_0^2 \gg 1$, the dependence of tSNR on image SNR weakens and tSNR eventually saturates at a limiting value of $\mathrm{tSNR} = 1/\lambda$. This is the case that applies for the moderate resolution scans used in most fMRI studies in which the signal dependent term σ_p dominates the signal independent noise term σ_T. When operating in this regime, increases in image SNR (e.g. due to an increase in magnetic field strength) have a diminishing effect on tSNR (Triantafyllou et al., 2005). The dependence of tSNR on voxel volume is discussed further in Section 2.4.

2.1. Background noise

The background noise term $n(t)$ in Eq. (3) reflects the contributions of sources that are independent of the signal of interest. This includes thermal noise arising from the thermal agitation of charge carriers in both the subject and the MRI system electronics. For the modern systems and field strengths used in most fMRI studies, the thermal noise term is typically dominated by the subject noise contribution (Edelstein et al., 1986). The background noise also includes other sources of radiofrequency (RF) noise, such as RF spikes due to intermittent mechanical contacts between metal components and spurious RF noise from the environment (e.g. commercial radio signals that leak through a magnet room's RF shield) (Greve et al., 2011). The background noise term is present even if there is no activity-related signal of interest. Indeed, one way to measure the background noise is to simply acquire the data without exciting any magnetization. This is done by setting the flip angle of the RF excitation pulse to zero, such that $S_0(t) = 0$ and therefore $S(t) = n(t)$.

The presence of RF spikes and interference is considered undesirable for a well operating MRI system and much engineering effort goes into minimizing these noise sources. On the other hand, thermal noise is always present. However, since it is a wideband noise source (i.e. equal power at all temporal frequencies), its effects can be reduced through filtering to eliminate noise from frequencies that are outside of the signal band of interest. This is accomplished in the acquisition process through the use of low-pass filters in the signal processing chain (e.g. by setting the receiver bandwidth to an appropriate value). Further filtering is performed during the processing and reconstruction of images from the acquired raw MRI data. Because MRI acquires data at different spatial frequencies as a function of time, wideband noise in the temporal frequency domain is transformed into wideband noise in the spatial frequency domain (Nishimura, 2010). Noise outside the spatial frequencies of interest can therefore be directly filtered out in the spatial frequency domain (known as k-space filtering) or in the image domain through convolution with a low-pass spatial filter (e.g. smoothing of the images).

2.2. Noise in the magnetization term

The $\frac{\Delta S_0(t)}{S_0(0)}$ term reflect temporal changes in the initial transverse magnetization $S_0(t)$ that is created by the RF excitation pulse at the start of each repetition. Noise sources in this term include both MRI system-related instabilities and physiological noise components. In an ideal MRI system, all of the RF and gradient pulses are played out perfectly across time. For example, if the user specifies

an excitation pulse with a flip angle of 90°, then the ideal RF system would execute a perfect 90° flip angle pulse across all repetitions. However, in practice there can be variations in the flip angle over time that result in corresponding variations in the excited magnetization. In the gradient system, instabilities and imperfections can lead to variations in the spatial frequency components that are acquired over time, leading to temporal variations in the reconstructed images. In a similar fashion, heating of the ferromagnetic elements in the passive shim system can reduce their magnetization, leading to changes in the overall magnetic field that result in time-varying distortions and shifts of the acquired images (Foerster et al., 2005). For a well designed and maintained MRI system, the goal is to minimize system instabilities so that they constitute a relatively minor contribution to the overall noise (Glover et al., 2012; Liu et al., 2015).

Physiological processes that can give rise to changes in magnetization include subject motion, cardiac pulsations, and respiratory activity. These processes lead to variations in the measured magnetization by directly altering the tissue composition in each voxel (e.g. due to motion or displacement) or by affecting the magnetic field environment. For example, magnetic field fluctuations due to respiratory and cardiac activity can cause temporal variations in magnetization by perturbing the process of steady-state free precession for acquisitions with relatively short repetition times (e.g. 200 ms), such as the multiband acquisitions discussed below in Section 3.1 (Zhao et al., 2000). The various underlying mechanisms are discussed in more detail in Section 3. The magnetization can also be affected by in-flow effects whereby an increase in cerebral blood flow increases the number of spins that flow into an imaging voxel (Gao and Liu, 2012). As these flowing spins have not experienced the same number of RF pulses as the static tissue, an increase in their number leads to an increase in the excitable magnetization. Although this is a functionally related change, some studies aim to minimize this effect so as not to confound the in-flow changes with the pure BOLD effect. This can be done by increasing the repetition time (TR) or reducing the flip angle. Alternatively, multi-echo acquisitions can be used to differentiate in-flow and BOLD effects (Glover et al., 1996; Speck and Hennig, 1998; Menon et al., 1993).

2.3. Noise in the relaxation term

Noise in the $TE{\cdot}\Delta R_2^*(t)$ term reflects sources that modulate the relaxation rate $R_2^*(t)$ in a way that may not be directly related to the neural activity of interest. As the relaxation rate that is of interest in BOLD fMRI studies depends on the total amount of deoxyhemoglobin (dHB) in the blood, this rate is sensitive to factors that alter cerebral blood flow and metabolism. The primary physiological sources are: (1) modulation of cerebral blood flow through variations in respiratory activity; (2) variations in the cardiac rate that can modulate cerebral blood flow, volume, and oxygenation, and (3) processes that give rise to intrinsic fluctuations in blood flow and metabolism, including variations in blood pressure and resting-state neural activity. The relaxation term can also be modulated by dynamic fluctuations in the magnetic field, due for example to respiratory activity. These sources are discussed in more detail in Section 3.

2.4. Relative contribution of noise sources

Because they have different signal dependencies, the relative contribution of the noise sources in Eq. (3) can be assessed using various experimental manipulations (Greve et al., 2011; Krüger and Glover, 2001). For example, as mentioned above, the background noise can be measured by setting the flip angle to zero. Alternatively, the signal can be measured across a range of non-zero flip angles, and the value of the signal at zero flip angle can be extrapolated. Weisskoff (1996) noted that the impact of system instabilities could be differentiated from background noise by measuring the tSNR as a function of the size of region of interest (ROI). When only thermal noise components are present, the tSNR increases as the square root of the number of voxels in the ROI, and any deviations from this expected relation are indicative of non-thermal noise contributions. The non-BOLD and BOLD-like components in Eq. (3) can be distinguished using a multi-echo acquisition and taking advantage of the fact that the BOLD-like component has a linear dependence on echo time.

Studies that have used these approaches to characterize noise have found that physiological and thermal noise components dominate at the typical field strengths and parameter values used in fMRI studies (Greve et al., 2011; Krüger and Glover, 2001; Triantafyllou et al., 2005). For example, Greve et al. (2011) found that system instabilities were generally less than 2% and 10% of the physiological noise levels in gray and white matter, respectively, at a magnetic field strength of 3 Tesla and spatial resolution of 3.44 mm × 3.44 mm × 4 mm. In contrast, the background noise was found to constitute a significant portion of the overall noise variance, with levels ranging from 40% to 90% of total variance in white matter and 10% to 50% of total noise variance in gray matter. Because physiological noise is signal dependent (as reflected in the presence of the $S(0)$ term in Eq. (2)), its relative contribution will decrease as the voxel volume is reduced. Bodurka et al. (2007) found that at 3 T the physiological and background thermal noise contributions were approximately the same for a voxel volume of 1.8 mm^3 in gray matter and 2.1 mm^3 in white matter. As voxel volume is further decreased, thermal noise becomes the dominant source of noise, so that increases in image SNR (e.g. due to an increase in magnetic field strength) can translate into improvements in tSNR (Triantafyllou et al., 2005). This corresponds to the small image SNR regime (see Eq. (5)) in which tSNR exhibits a linear dependence on image SNR. For larger voxel volumes, physiological noise is expected to dominate, such that there is a range of signal levels over which decreases in the signal-dependent physiological noise will not greatly affect tSNR. It has been suggested that in this regime a lower flip angle can be used to reduce the physiological noise component while maintaining a reasonable tSNR level (Gonzalez-Castillo et al., 2011). In certain brain regions, such as the brainstem, the proximity to large vessels and fluid-filled spaces leads to a higher relative contribution of physiological noise (Brooks et al., 2013).

3. Physiological noise sources

The presence of physiological noise sources was noted very early in the history of fMRI in a seminal abstract by Weisskoff et al. (1993) with the compelling subtitle “What's in the Noise?”. By acquiring a single slice of data from the visual cortex at a short repetition time (TR = 133 ms), Weisskoff and colleagues were able to characterize the noise power spectrum up to a frequency of 3.5 Hz. For the spectrum within gray matter they observed a strong peak close to the typical cardiac heart rate (about 1 Hz). This cardiac peak was also observed in the spectra from the ventricles and sagittal sinus. In addition, these regions showed a peak near the respiratory rate (about 0.25 Hz). At very low frequencies (less than 0.25 Hz), the spectrum in gray matter showed an increase in power as compared to the spectrum in white matter. In many ways, the observations in this one-page abstract delineated the basic themes of several areas of investigations that continue to this day. In particular, the investigation of low frequency fluctuations would later blossom into the field of resting-state fMRI.

3.1. Cardiac noise sources

The primary source of cardiac-induced signal change is thought to be cardiac pulsations which lead to dynamic changes in the relative distribution of brain tissue, blood, and cerebrospinal fluid (Dagli et al., 1999; Hu et al., 1995; Bhattacharyya and Lowe, 2004). Pulsation-related artifacts tend to be most pronounced near the large arteries (Dagli et al., 1999; Glover et al., 2000; Restom et al., 2006). When the sampling rate is high enough, cardiac-related contributions are easily visible in the fMRI signal spectra near the cardiac rate (Weisskoff et al., 1993; Frank et al., 2001; Biswal et al., 1996). In addition, with recently developed short TR whole brain multiband echoplanar imaging acquisitions, the dynamic passage of the cardiac-related pulsations through the brain can be visualized (Tong et al., 2014). However, for the typical TRs used in fMRI experiments, cardiac pulsations are undersampled and appear at an aliased frequency. For example, with a TR of 2.5 s, the sampling rate is 0.4 Hz and a cardiac signal with a true frequency of 1 Hz will appear at a frequency of 0.2 Hz. As mentioned above, multiband acquisitions can provide TRs short enough (e.g. 400ms) to avoid aliasing at lower spatial resolutions, but for higher spatial resolutions, such as the 2 mm isotropic resolution used for the Human Connectome Project (Smith et al., 2013), the TR that can be achieved (on the order of 700–800 ms) with currently available MRI hardware is not sufficient to avoid aliasing of the cardiac signal.

When the cardiac signal is aliased it can overlap in the frequency domain with signals of interest, such as task-related activations or functional resting-state fluctuations, thereby complicating the identification of the cardiac noise contribution. To address this issue, retrospective methods have been developed to better identify cardiac noise sources (Glover et al., 2000; Hu et al., 1995). In these methods, an external measurement of cardiac activity is acquired (typically with a pulse oximeter) and the data is sorted with respect to its relation to the cardiac phase. For cases where an external measure is not available, an estimate of the cardiac noise contributions can be obtained from regions in which the signal is likely to be dominated by physiological noise, such as the large vessels, white matter, and ventricles (Behzadi et al., 2007; Lund et al., 2006). However, emerging work regarding the potential detection of functional signals in white matter suggest that some level of caution may be needed when using white matter signals as proxies for noise (Gawryluk et al., 2014).

In addition to the direct effect of cardiac pulsations, fluctuations in the cardiac rate have been shown to be significant sources of variation in the fMRI signal (Chang et al., 2009; Shmueli et al., 2007). As the BOLD fMRI signal is a complex function of changes in cerebral blood flow, volume, and oxygenation (Buxton et al., 2004), it has been proposed that the observed effects reflect low frequency changes in the cerebrovascular system driven by heart rate variations. Respiratory modulation of the heart rate is a well characterized phenomenon (known as respiratory sinus arrythmia) in which the heart rate increases during inspiration and decreases during expiration (Berntson et al., 1993). It is likely that a portion of the rate-related changes are due to this effect (Chang et al., 2016). Indeed, Frank et al. (2001) noted the presence of respiratory sidebands that surrounded the cardiac peak in fMRI data, where the sidebands were offset from the peak frequency by the fundamental frequency of the respiratory noise peak.

3.2. Respiratory noise sources

A number of potential mechanisms have been proposed to account for the effect of respiratory activity on the fMRI signal. With breathing, there are expansions and contractions of the chest cavity and walls that lead to dynamic variations in bulk magnetic susceptibility and related perturbations of the main magnetic field. These field changes then give rise to phase differences that result in shifts and distortions in the acquired images that vary across both space and time (Brosch et al., 2002; Raj et al., 2001). In addition, the field perturbations can modulate the degree of intervoxel dephasing and cause changes in the effective relaxation rate (Raj et al., 2001). Mechanisms that lead to changes in the magnetization term include bulk motion of the head related to the action of breathing and brain tissue deformation due to venous pressure changes during respiration (Hu et al., 1995; Windischberger et al., 2002). Susceptibility and bulk motion related effects tend to be spread over the entire brain whereas tissue deformation effects tend to be more localized (Glover et al., 2000; Hu et al., 1995).

Respiration can exert an indirect effect on the fMRI signal through its modulation of carbon dioxide (CO_2) levels. Carbon dioxide is a potent vasodilator, and therefore fluctuations in CO_2 levels can lead to dynamic variations in cerebral blood flow. These fluctuations occur at low frequencies in the range of 0.0 to 0.05 Hz, as compared to the typical respiratory frequency range of 0.1–0.3 Hz (Wise et al., 2004). In addition, the effects are significantly greater in gray matter as compared to white matter, and there is regional heterogeneity in the size of the effect in gray matter, possibly reflecting variations in the vascular response to CO_2. The latency between end-tidal CO_2 fluctuations and the associated BOLD response appears to be longer when subjects have their eyes closed, as compared to the eyes open condition (Peng et al., 2013).

Noting the relation between inspired respiratory volume and endtidal CO_2, Birn et al. (2006) explored the relation between the BOLD signal and a measure of respiration per volume time (RVT), defined as the ratio of the depth of breathing to the period of respiration. Consistent with the prior findings that used endtidal CO_2 measures, they found a significant relationship between RVT and the BOLD signal, which was particularly strong in gray matter regions. In addition they found that the RVT-related changes were found to be pronounced in regions associated with the default mode network (DMN), which in some cases complicated the ability to distinguish functional resting-state activity in the DMN from respiratory activity (Birn et al., 2006, 2008a).

3.3. Low frequency drifts and fluctuations

Since the initial observations of Weisskoff et al. (1993), the existence of low-frequency signal drifts and fluctuations has been consistently observed, with an inverse relation between spectral power and frequency (Zarahn et al., 1997; Purdon and Weisskoff, 1998). Because these low frequency components can occupy the same frequency band (roughly 0.0–0.1 Hz) as task-related fMRI block designs, their presence can bias the detection of functional activations (Aguirre et al., 2002; Purdon and Weisskoff, 1998). For example, as discussed in more detail in Section 6.1.1, the presence of low frequency confounds can lead to a reduction in sensitivity when these confounds are included as structured noise components in an analysis model. Because of this effect, low frequency task designs (e.g. with epochs longer than 60 s) are not typically used in BOLD fMRI studies. For low-frequency task designs, arterial spin labeling (ASL) fMRI has been shown to provide better performance than BOLD fMRI due to the inherent minimization of low frequency confounds in the acquisition and processing of ASL data (Aguirre et al., 2002; Wang et al., 2003b, 2003a; Liu and Wong, 2005). However, recent work using a multi-echo approach to separate BOLD-like from non-BOLD-like low-frequency fluctuations suggests that low-frequency task designs may be practical for BOLD fMRI studies when the appropriate acquisition and analysis schemes are employed (Evans et al., 2015).

A portion of the low frequency drift has been shown to come

from scanner instabilities, with more pronounced effects for regions with high spatial intensity gradients (Smith et al., 1999). For example, the slow drift in the shim system that was discussed in Section 2.2 could cause slow spatially varying distortions and shifts in the image over time that would manifest as signal drifts within individual voxels. To ensure that the effect of scanner instability is minimized for fMRI studies, the characterization of scanner drift plays a key component in the fMRI system quality assurance process (Liu et al., 2015; Friedman and Glover, 2006).

As noted in the early work of Weisskoff et al. (1993), the presence of low-frequency fluctuations is greater in gray matter as compared to white matter, suggesting that physiological fluctuations as opposed to system instabilities (which would tend to produce uniform effects across both tissue types) are the primary source of the observed signals. Using measurements over a range of flip angles and echo times, Yan et al. (2009) demonstrated that a significant portion of the low-frequency fluctuations exhibited BOLD-like contrast, most likely reflecting intrinsic fluctuations in blood flow and metabolism. It is these fluctuations that form the basis for the field of resting-state fMRI, which began with the seminal paper of (Biswal et al., 1995) that first described the presence of functionally related spatial correlations in resting-state BOLD fMRI data. Fluctuations in the 0.0–0.1 Hz frequency band have been shown to account for about 90% of the observed connectivity strength (Cordes et al., 2001). Signals within the 0.01–0.1 Hz band have been found to correspond to localized functional networks whereas signals in the 0.0–0.01 Hz band were associated with more widespread global correlations (Yan et al., 2009). The signal components in this lower frequency band (0.0–0.01 Hz) are often considered to be nuisance drift components and are removed with either high pass filtering or the inclusion of low-frequency drift terms as regressors in the analysis process (see Section 6.1.2).

The ability of resting-state fMRI to non-invasively characterize the functional connectivity of the brain has led to its adoption in a wide range of studies, including a number of large scale projects, such as the Human Connectome Project (Fox and Raichle, 2007; Smith et al., 2013). The standard deviation (and related measures) of the resting-state fluctuations has also proven to be a useful metric of brain activity (Zou et al., 2012; Wong et al., 2014). For example, Zou et al. (2012) found that the amplitude of low-frequency fluctuations was predictive of working memory performance. While the origins of the resting-state BOLD fluctuations are still not completely understood, there is growing evidence supporting a strong link between the resting state BOLD fMRI measures and eletroencephalographic and magnetoencephalogrphic measures of brain activity (Brookes et al., 2011; Yuan et al., 2016; Tagliazucchi et al., 2012; Goldman et al., 2002). However, the potential contribution of low-frequency fluctuations of non-neuronal origin must still be considered (Tong et al., 2015; Tong and Frederick, 2014).

Low-frequency fluctuations and resting-state fMRI represent an interesting case in which a component that was originally considered noise became a signal of great interest. Indeed, from the standpoint of task-related fMRI, the low-frequency fluctuations may still be considered noise because the background fluctuations can mask the detection of subtle low-amplitude functional activations. On the other hand, it has been shown that intrinsic fluctuations can modulate the amplitude of task-related responses across trials (Fox et al., 2007; Mayhew et al., 2016). Thus, even within the context of task-related fMRI, it is important not to lose sight of the intrinsic fluctuations as a potential signal of interest.

4. Motion

4.1. Effects of motion on the fMRI signal

Since the early days of fMRI, motion has been recognized as a significant source of artifactual signal changes (Hajnal et al., 1994). In an ideal fMRI acquisition, the signal acquired over time from a voxel is treated as a faithful representation of the BOLD-related activity from a specific point in space. When a subject moves within the scanner, the signal deviates from this ideal representation. For example, if the motion is such that the subject moves by the width of one voxel exactly halfway during the scan, the acquired time series will represent the MRI signal from one voxel during the first half of the scan and from the neighboring voxel during the latter half. In reality, the situation is more complex, and the measured signal is a time-varying combination of the signals from a neighborhood of voxels. The signal changes are especially pronounced when there is a large difference in signal intensity between neighboring voxels, for example at the interface of brain tissue and cerebral spinal fluid. It is the relative displacement (e.g. motion between volumes) rather than the absolute displacement (i.e. from an initial reference point) that gives rise to the most pronounced motion-related BOLD signal changes (Power et al., 2015).

In addition to the first order effects of motion, there are also complex spin-history effects that arise when there is movement across slices during the course of a scan (Friston et al., 1996). In a 2D MRI acquisition scheme, slice-selective RF pulses are used to excite the magnetization on a per-slice basis with various slices excited at different points within a repetition interval. In the absence of movement, the spins in a given brain region are excited at regular time intervals (i.e. once per repetition), such that the time for saturation recovery of the spins is constant across the scan. When there is movement, a brain region may move between excited slices such that the spins are no longer excited at regular intervals. This can lead to changes in the MR signal due to differences in the saturation recovery of the spins.

An additional source of motion-related artifacts reflects deviations from ideal behavior in the magnetic fields used in fMRI acquisitions – i.e. the static magnetic field and the RF field are not uniform and the gradient fields are not perfectly linear. As spins are translated via motion into different portions of these non-ideal fields, the interaction between the spins and fields varies across time, giving rise to changes in the acquired images. For example, strong-susceptibility gradients around the sinuses are known to cause significant distortions in fMRI images (Andersson et al., 2001). These distortions arise because the actual magnetic field experienced by a spin differs from the assumed field, and thus the position of the spin is displaced in the reconstruction process. With motion, the amount of displacement can vary with time as a spin moves into different parts of the non-uniform magnetic field. In addition, the distribution of the magnetic field changes as the position of the head moves with respect to the main magnetic field. Both these factors result in time-varying distortion of the acquired images (Jiang et al., 1995). While the effects of distortion can be greatly reduced through the application of image distortion correction methods (Andersson et al., 2003), the remaining distortions will still manifest as motion-related noise. In addition, the very process of distortion correction can be complicated by motion because the calibration scans used in the process are typically acquired before or after the scan. Thus, any motion between the calibration scan and the image of interest will tend to reduce the effectiveness of the correction process.

4.2. Mitigating the effects of motion

The primary effects of motion (e.g. spatial misalignment between acquired images) are typically addressed with retrospective image registration algorithms that are a standard feature of fMRI processing and analysis pathways. However, as mentioned above, the ability of these retrospective approaches to deal with susceptibility-related signal changes can be limited. Prospective motion correction methods have been developed to minimize the effects of motion by having the acquisition process track the motion in real-time (Maclaren et al., 2013). In addition to minimizing the first order effects of motion, the prospective approach can also reduce spin-history effects, since the positioning of the excitation slices can be adjusted to match the motion (Yancey et al., 2011). Prospective motion correction can also facilitate the correction of dynamic variations in susceptibility-related distortion. With prospective correction, the orientation of the head remains relatively constant with respect to the phase-encode direction (which is the main direction for distortion), thus simplifying the distortion correction procedure (Ooi et al., 2013).

In considering the effects of motion, there is an important distinction between task-related and resting-state fMRI studies. For task-related studies, subject motion is often found to be correlated with the stimulus (Hajnal et al., 1994), whereas for resting-state fMRI studies there is not an explicit time-varying task. In task-based fMRI, image registration software can be used to reduce some of the effects of task-related motion, but there are residual effects due to the imperfect nature of the registration process, including limitations in the ability to address spin-history and distortion effects (Johnstone et al., 2006). To deal with these residual effects, estimates of the motion are often used as nuisance regressors in the statistical analysis of the data, including 6 motion estimates (3 translation parameters and 3 rotation parameters) and functions of these estimates, such as the temporal derivatives of the motion estimates and the framewise displacement (Power et al., 2015). The motion estimates can be obtained from the image registration process, external (e.g optical or EEG-based) measures of the motion, or images acquired at a short echo time (Bright and Murphy, 2013; Buur et al., 2009; Wong et al., 2016). When nuisance regressors were included in studies with a block design, even fairly moderate (e.g. $r \approx 0.2$) correlations between the task and motion covariates led to significant decreases in the ability to detect functional activations (Johnstone et al., 2006). In contrast, for event-related designs, the inclusion of covariates improved detection sensitivity, reflecting the low correlation between the motion parameters and the design model. Additional discussion on the use of regressors is provided below in Section 6.1.1. As an alternative to the use of motion regressors, censoring or "scrubbing" of high motion volumes has been proposed, with one study reporting that censoring outperformed the use of motion regressors (Siegel et al., 2014).

The procedures described for task-related fMRI studies, such as image registration, nuisance regression, and scrubbing, are equally applicable to resting-state studies, where motion has been shown to have a major effect on estimates of functional connectivity (Power et al., 2012; Satterthwaite et al., 2012; Van Dijk et al., 2012). Because motion-related variance tends to be similar for neighboring voxels, the presence of motion can lead to an overestimation of the strength of near-range connections as compared to long-range connections. As a result, a high-motion group (such as children) would tend to exhibit stronger near-range connections than a low motion group, with the potential for weaker long-range connections in the high-motion group (Power et al., 2015). However, a recent study suggests that caution must be used when attributing differences in connectivity solely to differences in motion. In a study comparing inter-subject versus intra-subject differences in motion and functional connectivity, Zeng et al. (2014) found evidence for a stable neurobiological trait, marked by reduced long-range connections in the default mode network, that was associated with the predisposition for movement. As this trait was observed across both low-motion and high motion scans of the same subject, the findings suggest that motion-related differences in connectivity may partly reflect non-artifactual differences in the underlying neurobiology.

5. The global signal

The term global signal does not refer to any specific noise source, but rather represents a "catch-all" signal that captures the influence of a variety of noise components. It is defined as the mean time course computed over all voxels within the brain (although sometimes limited to gray matter) (Zarahn et al., 1997). As it is a time-varying spatial average, it is useful for representing the influence of spatially coherent noise sources, such as physiological noise and motion. The global signal has been used as a covariate to remove the effects of noise in the analysis of task-based fMRI studies (Zarahn et al., 1997; Aguirre et al., 1997, 1998; Macey et al., 2004). When there is a strong correlation between the global signal and the task design, its inclusion as a covariate can significantly alter the analysis results (Aguirre et al., 1998). Overall, the use of the global signal in the analysis of task-related studies has been rather moderate in scope. In contrast, the global signal has been widely adopted as a covariate in the analysis of resting-state fMRI studies. In a pre-processing step commonly referred to as global signal regression (GSR), the global signal is regressed out of all voxel time series prior to the computation of correlations. It has been shown that GSR can be effective for removing motion artifacts (Power et al., 2015) and greatly improves the quality of resting-state correlation maps (Fox et al., 2009; He and Liu, 2012). However, GSR is highly controversial, as its use can potentially introduce artifactual negative correlations (Murphy et al., 2009; Fox et al., 2009). There is also growing evidence that the global signal does not just contain noise. For example, studies using simultaneous EEG and fMRI measures have demonstrated a relation between the global signal and EEG measures of vigilance and broadband neuro-electrical activity (Wen and Liu, 2016; Wong et al., 2013). In addition, features of the global signal have been shown to distinguish subjects with schizophrenia from healthy controls (Yang et al., 2014; Hahamy et al., 2014). Thus, the existing evidence suggests that the global signal is best viewed as containing both meaningful signals of interest and noise components.

6. Separating signal from noise

In the prior sections, we have already mentioned some of the specific methods that have been used to separate signal from noise in fMRI studies. Here we take a closer look at the two main approaches. In the first approach, we explicitly model the characteristics of the signal and noise components using the framework of the general linear model (GLM). In this framework, both our assumptions and any available information about the signal and noise are encoded into the model (Lund et al., 2006). The signal and noise parameters are then simultaneously estimated in a manner that provides the best fit of the model to the observed data. In the second approach, a data-driven analysis method, such as independent components analysis, is used to factor the data into a set of components, where the factorization aims to optimize a predefined criterion, such as the statistical independence between components. Once the components have been computed, a second step is required to differentiate signal from noise components.

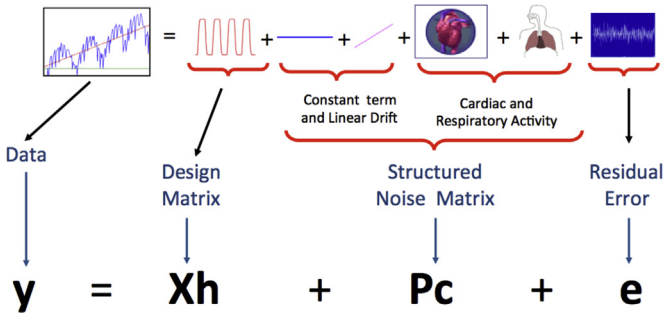

Fig. 1. Diagram of general linear model (GLM) for fMRI data. The measured data **y** is the sum of a signal of interest **Xh**, structured noise components **Pc**, and residual error **e**. The design matrix **X** encodes information about the experimental stimulus while the structured noise matrix **P** contains information about the noise sources. The model parameters **h** and **c** are determined by fitting the model to the data. Examples of the types of signals that are used as columns in **X** and **P** are shown. Additional noise components that can be included in **P** are discussed in the text.

6.1. Model-based approaches

6.1.1. The general linear model

In the GLM for fMRI data, the measured signal **y** is represented as the sum

$$\mathbf{y} = \mathbf{Xh} + \mathbf{Pc} + \mathbf{e} \tag{6}$$

of desired signal components **Xh**, structured noise components **Pc**, and a residual error term **e**, where **X** is the experimental design matrix, **h** is a vector of unknown hemodynamic parameters, **P** is a matrix of structured noise regressors (also referred to as nuisance regressors), and **c** is a vector of noise regressor weights. The residual term represents the portion of the signal that cannot be explained by either the desired signal or structured noise components, and includes random noise contributions (e.g. thermal noise) and noise sources that have not been identified or modeled correctly. Statistical structure in this residual term is typically modeled using a covariance matrix. A schematic diagram of the GLM is presented in Fig. 1.

For task-related fMRI experiments, the design matrix **X** encapsulates information about the stimulus, such as the timing, strength, and type of the stimulus events. The columns of the matrix **P** represent both prior assumptions and information about structured noise sources, which include low-frequency drifts, physiological noise components, and motion-related artifacts. Statistical analysis of an experiment entails first estimating the model parameters **h** and **c** that provide the best fit to the measured signal. A test statistic is then formed by first determining the portion of the data **y** that can be explained by the part of the signal space (spanned by the columns of **X**) that is orthogonal to the nuisance subspace (spanned by the columns of **P**) and then comparing this to the magnitude of the residual term **e** (Liu et al., 2001). In other words, the test statistic focuses on the fraction of the measured data that can be explained only by the desired signal model and not by the structured noise model. If there is a large overlap between the spaces spanned by the two models, then this fraction can be greatly diminished, reducing the sensitivity of the experiment (Liu et al., 2001). Overlap can occur when the task itself induces structure-related noise components, such as task-correlated motion and changes in respiratory and cardiac activity (Johnstone et al., 2006; Birn et al., 2009). An overlap can also occur when the frequency of the task lies within the band of the low-frequency nuisance terms. For resting-state fMRI studies, there is no explicit design matrix, and the model reduces to $\mathbf{y} = \mathbf{Pc} + \mathbf{e}$, where the residual term **e** that remains after regressing out structured noise terms becomes the signal of interest.

6.1.2. Modeling of structured noise components

Low frequency drifts are often represented by Legendre polynomials (e.g. linear and quadratic terms) or low-frequency sine and cosine terms (Friston et al., 1995; Cox, 1996). For physiological noise regressors, measures of cardiac and respiratory activity are typically obtained using a pulse oximeter and a respiratory effort transducer, respectively, which are standard pieces of equipment on most modern MRI systems. Measures of end-tidal CO_2 can also provide an index of respiratory activity, but are not always available as part of the standard system environment. A recent study has shown that an in-bore MRI-compatible camera has the potential to provide contact-free measures of both cardiac and respiratory fluctuations, although the robustness of the method to motion has not been fully characterized (Maclaren et al., 2015).

Once cardiac and respiratory measures have been obtained, physiological noise regressors reflecting the primary and secondary effects of the sources can be formed. For the primary effects, the regressors are based on the phase of the cardiac and respiratory measures, (Glover et al., 2000; Hu et al., 1995; Josephs et al., 2007). When the regression is performed in k-space, the method is referred to as RETROKCOR (Hu et al., 1995), whereas in image space the method is known as RETROICOR (Glover et al., 2000). As most fMRI studies do not have easy access to the k-space data, the RETROICOR approach is more widely used in practice. In addition, as it is image-based, RETROICOR can be more effective in identifying spatially localized effects. Extensions to RETROICOR include its application to arterial-spin labeling (ASL) based fMRI (Restom et al., 2006), where the removal of physiological noise is especially critical given the low intrinsic sensitivity of the ASL acquisition method. Särkkä et al. (2012) proposed a dynamic version of RETROICOR to better handle time-varying changes in the amplitude and frequency of physiological fluctuations. In addition, it should be noted that many fMRI acquisition protocols use navigator echoes to measure and dynamically correct for global phase shifts as part of the image acquisition and reconstruction process (Pfeuffer et al., 2002).

For the secondary effects of respiration, the RVT regressor described above can be included as a regressor after convolution with a respiratory response function as proposed by Birn et al. (2008b). In a similar fashion, Chang et al. (2009) proposed the use of the cardiac rate after convolution with a cardiac response function. Analytic expressions for the respiratory and cardiac response functions (based on subject average responses) are provided in Birn et al. (2008b) and Chang et al. (2009), and the use of the associated regressors is referred to as RVHRCOR (Chang and Glover, 2009). As an alternative to the analytic expressions, Falahpour et al. (2013) have shown that subject-specific respiratory and cardiac response functions derived from the global signal can account for inter-subject differences in the physiological responses. However, inter-scan variability in the derived estimates may represent a practical limitation to this approach.

While the use of external measures of physiological activity is considered a best practice for fMRI studies, these measures are not always acquired. In addition, the quality of the measures can vary greatly across subjects, scans, and facilities, due to factors such as subject motion and equipment malfunctions, sometimes rendering the measures unusable. If the repetition time is short enough to avoid aliasing of the cardiac and respiratory signals, these can be directly estimated from the image data and used to form physiological noise regressors (Chuang and Chen, 2001; Le and Hu, 1996). As mentioned previously, estimates obtained from large vessels, white matter, and the ventricles have been proposed as a proxy for external physiological measures (Behzadi et al., 2007; Lund et al., 2006; Curtis and Menon, 2014; Bianciardi et al., 2009; Jo et al., 2010. For example, in the aCompCor method (Behzadi et al., 2007), an anatomical mask is used to define regions that

consist almost entirely of either white matter or cerebrospinal fluid, a principal components analysis is performed on the time series in each region, and the top components are then selected as noise regressors. Because they do not require external physiological measures, data-driven methods such as aCompCor are finding increasing use, especially for resting state fMRI studies.

As noted above in Section 4.2, regressors for motion are typically derived from the image registration process. However, even when a large number (e.g. 36) of motion regressors are used, a significant amount of motion-related artifacts can still be observed in the data (Power et al., 2015). Bright and Murphy (2015) found that there were limited gains in performance when more than 6 motion regressors were used. They also found that the structured noise components identified when a large number of regressors was used exhibited network structures similar to "true" functional networks, suggesting that with the extra degrees of freedom the model was also fitting a significant fraction of the true functional signal. In comparing motion regression versus censoring, Siegel et al. (2014) reported that censoring provided better performance. However, Muschelli et al. (2014) found that regression performed well when a combination of motion regressors and principal components derived from nuisance regions was used, and there was no added benefit from censoring. They also reported that the use of principal components provided greater performance than the use of mean signals from the nuisance regions, partly reflecting the fact that component-based approaches can preserve information that may otherwise be averaged out when using the mean signal. Similarly, Patriat et al. (2015) found that a principal component based regression approach provided gains in performance even after the data had been censored.

6.1.3. GLM versus preprocessing

As a cautionary note, although the discussion above has the used the framework of the GLM in Eq. (6) to discuss the separation of signal from noise, this approach is not always used. Instead, the removal of the structured noise terms is sometimes treated as a pre-processing step prior to the statistical analysis of the data (Glover et al., 2000; Chang and Glover, 2009). The GLM and preprocessing approaches provide identical parameter estimates when the desired signal regressors are orthogonal to the structured noise regressors. However, when the two sets of regressors are not orthogonal, the parameter estimates and associated statistics computed after preprocessing will differ from those using the GLM approach (Liu et al., 2001). In addition, when using the GLM, the number of noise regressors will reduce the degrees of freedom assigned to the residual term, whereas this reduction in degrees of freedom is not incurred if the regression is considered a pre-processing step. As with many issues in fMRI, there is not a great deal of consistency with regards to how pre-processing approaches are handled in the statistical analysis and interpretation of the data. In some cases, the noise correction is an integrated part of the acquisition and reconstruction process, such as the dynamic correction of respiratory field changes (Pfeuffer et al., 2002) or the use of prospective motion correction. For these cases, there is not necessarily a straightforward way of taking into account the preprocessing into the analysis process. On the other hand, when all the available data are used to form estimates of the model parameters, then an argument can be made that the GLM approach is preferred to a two-step process. Nevertheless, further studies along the lines of Churchill et al. (2015) are needed to better understand the impact of the various approaches.

6.2. Data driven approaches

In discussing the model-based approach, we have already touched upon the use of principal components analysis (PCA), which is a widely used method for finding structure in data, to estimate noise components from pre-specified nuisance regions. In fully data-driven approaches, there is no explicit model for the structured noise. Instead algorithms, such as PCA or independent components analysis (ICA), are used to first decompose the data into a set of components, followed by a second step to distinguish signal components from noise components. While PCA has been used for the analysis of fMRI data (Thomas et al., 2002), its main use now is as a preprocessing step to reduce data dimensionality prior to the application of ICA.

ICA is a type of blind source separation that does not require the user to specify a priori information about either the signals of interest or the noise components. Instead, it uses higher order statistics to maximize the statistical independence of the components (Bell and Sejnowski, 1995). McKeown et al. (1998) introduced ICA into the field of fMRI and showed that the method could separate task-related components from noise-like components, such as those that exhibited the characteristics of head motion. Subsequent work showed that ICA could be used to successfully identify resting-state functional networks (Beckmann et al., 2005; Greicius et al., 2004). Resting-state fMRI is in many ways the ideal application for ICA because we know very little about the underlying signal sources. As a result, ICA has become one of the standard approaches for the analysis of resting-state fMRI studies.

In the context of fMRI, the independent components are spatial maps that are maximally independent, meaning that in the ideal case, knowledge about the amplitude of a given voxel in one spatial component map does not enable one to predict the amplitude for the corresponding voxel in another spatial component map. For each spatial component map, there is a corresponding time course, although there is no requirement that the component time courses are independent.

To distinguish signal from noise, investigators typically examine the spatiotemporal features (e.g. spatial smoothness, edge activity, temporal frequency content) of the spatial component maps and time courses (Rummel et al., 2013; Kelly et al., 2010; Bhaganagarapu et al., 2013). For example, a spatial component map that exhibits high amplitudes in voxels concentrated at the edges of the brain would typically be interpreted as a motion-related component. However, the identification of noise components can be highly subjective and requires a high level of experience and expertise. To address this issue, semi-automated or automated approaches have been proposed. For example, Thomas et al. (2002) based the identification of structured noise components on their spectral power in the cardiac and respiratory frequency bands, using data acquired with sufficient temporal resolution to avoid aliasing of the physiological noise sources. Perlbarg et al. (2007) identified noise components based on their ability to predict the fMRI signals from pre-defined regions, such as the ventricles and large vessels, that are thought to be dominated by physiological noise. Beall and Lowe (2007) used independent measures of physiological activity to identify ICA components that were correlated with the external measures and demonstrated that the resulting spatial maps could be used to estimate cardiac and respiratory activity. More recently, a number of groups have developed machine learning approaches in which human expertise is used to guide or train classification algorithms that automatically detect noise components based upon a set of spatiotemporal features (Salimi-Khorshidi et al., 2014; De Martino et al., 2007; Tohka et al., 2008; Sochat et al., 2014; Bhaganagarapu et al., 2013). A limitation of these approaches is the potential need to retrain the classifier if there are significant changes in the characteristics of the data (e.g. due to a change in the acquisition hardware or scan protocol). To address this limitation, Pruim et al. (2015b) introduced a method in which the features are largely

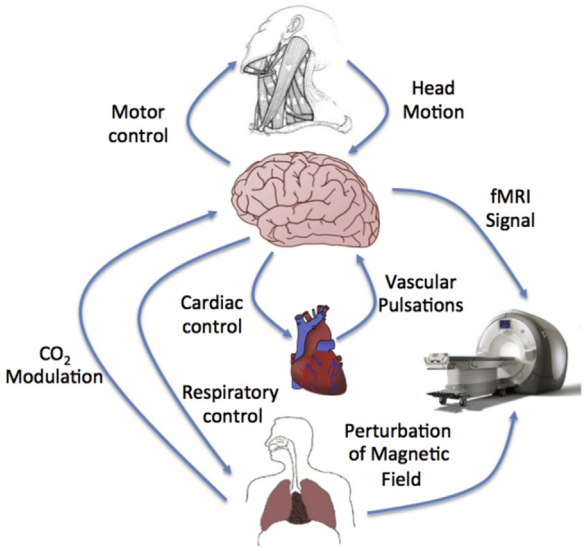

Fig. 2. Head motion, cardiac activity, and respiratory activity all contribute to noise in the fMRI signal. These functions are controlled by underlying brain activity, which generates BOLD fMRI signals of interest. As the brain can act as a common point of origin, the distinction between signal and noise is not always straightforward.

independent of the details of the acquisition process and have demonstrated its efficacy in reducing motion-related artifacts (Pruim et al., 2015a).

An alternative ICA-based approach takes advantage of multi-echo fMRI acquisitions and the linear dependence of the BOLD-like component on echo time. In the approach introduced by Kundu et al. (2012), the echo time dependence of independent components is used to distinguish between BOLD-like components (i.e. those components with voxel amplitudes that show a linear dependence on echo time) and non-BOLD-like noise components that do not exhibit a strong linear dependence. The method has been shown to be effective in automatically identifying components related to motion, physiological pulsations, and acquisition artifacts, such as those observed with multiband acquisitions (Olafsson et al., 2015). One potential limitation is that the characterization of components that show a small to moderate degree of linear dependence on echo time is not always straightforward, and the currently implemented algorithms rely on either ad-hoc or formal training using human experts to characterize components in this “gray” zone.

7. Conclusion

Efforts to characterize noise and mitigate its effects have played a key role in the development of fMRI. As the signal changes of interest can be relatively small, there has been concern from the early days of fMRI that noise sources, such as motion, could cause MRI signal changes that would be erroneously attributed to brain activity (Hajnal et al., 1994). Thus, efforts to understand the effects of noise have been critical for improving the analysis and interpretation of fMRI studies. However, as we have seen in this paper, the line between signal and noise is not always clear. A prime example of this ambiguity is the development of resting-state fMRI in which the signal of interest was once considered to be a primary source of noise (and can still be treated as a noise source in task-related fMRI analyses). The challenge in distinguishing signal from noise stems from the fact that the brain, which is the object of study, is the generator of both the signals of interest and noise. For example, as depicted in Fig. 2, noise fluctuations due to subject motion, respiration, and cardiac activity all have their origins in the brain networks that control these functions. Minimizing the contributions of these noise sources therefore risks the removal of information about the underlying brain activity (Iacovella and Hasson, 2011; Yuan et al., 2013). As fMRI continues to evolve it will be important for the field to remain mindful of this issue and to develop new analysis approaches that more effectively consider the interaction between signal and noise.

References

Aguirre, G.K., Zarahn, E., D'esposito, M., 1997. Empirical analyses of BOLD fMRI statistics. II. spatially smoothed data collected under null-hypothesis and experimental conditions. NeuroImage 5 (3), 199–212.
Aguirre, G.K., Zarahn, E., D'esposito, M., 1998. The inferential impact of global signal covariates in functional neuroimaging analyses. NeuroImage 8 (3), 302–306.
Aguirre, G.K., Detre, J.A., Zarahn, E., Alsop, D.C., 2002. Experimental design and the relative sensitivity of BOLD and perfusion fMRI. NeuroImage 15 (3), 488–500.
Andersson, J.L., Hutton, C., Ashburner, J., Turner, R., Friston, K., 2001. Modeling geometric deformations in EPI time series. NeuroImage 13 (5), 903–919.
Andersson, J.L.R., Skare, S., Ashburner, J., 2003. How to correct susceptibility distortions in spin-echo echo-planar images: application to diffusion tensor imaging. NeuroImage 20 (2), 870–888.
Beall, E.B., Lowe, M.J., 2007. Isolating physiologic noise sources with independently determined spatial measures. NeuroImage 37 (4), 1286–1300.
Beckmann, C.F., Deluca, M., Devlin, J.T., Smith, S.M., 2005. Investigations into resting-state connectivity using independent component analysis. Philos. Trans. R. Soc. Lond. Ser. B Biol. Sci. 360 (457), 1001–1013.
Behzadi, Y., Restom, K., Liau, J., Liu, T.T., 2007. A component based noise correction method (CompCor) for BOLD and perfusion based fMRI. Neuroimage 37 (1), 90–101.
Bell, A.J., Sejnowski, T.J., 1995. An information-maximization approach to blind separation and blind deconvolution. Neural Comput. 7 (6), 1129–1159.
Berntson, G.G., Cacioppo, J.T., Quigley, K.S., 1993. Respiratory sinus arrhythmia: autonomic origins, physiological mechanisms, and psychophysiological implications. Psychophysiology 30 (2), 183–196.
Bhaganagarapu, K., Jackson, G.D., Abbott, D.F., 2013. An automated method for identifying artifact in independent component analysis of resting-state FMRI. Front. Hum. Neurosci. 7, 343.
Bhattacharyya, P.K., Lowe, M.J., 2004. Cardiac-induced physiologic noise in tissue is a direct observation of cardiac-induced fluctuations. Magnet. Reson. Imag. 22 (1), 9–13.
Bianciardi, M., Van Gelderen, P., Duyn, J.H., Fukunaga, M., De Zwart, J.A., 2009. Making the most of fMRI at 7 T by suppressing spontaneous signal fluctuations. NeuroImage 44 (2), 448–454.
Birn, R.M., 2012. The role of physiological noise in resting-state functional connectivity. NeuroImage 62 (2), 864–870.
Birn, R.M., Murphy, K., Bandettini, P.A., 2008a. The effect of respiration variations on independent component analysis results of resting state functional connectivity. Hum. Brain Mapp. 29 (7), 740–750.
Birn, R.M., Diamond, J.B., Smith, M.A., Bandettini, P.A., 2006. Separating respiratory-variation-related fluctuations from neuronal-activity-related fluctuations in fMRI. NeuroImage 31 (4), 1536–1548.
Birn, R.M., Smith, M.A., Jones, T.B., Bandettini, P.A., 2008b. The respiration response function: the temporal dynamics of fMRI signal uctuations related to changes in respiration. NeuroImage 40 (2), 644–654.
Birn, R.M., Murphy, K., Handwerker, D.A., Bandettini, P.A., 2009. fMRI in the presence of task-correlated breathing variations. NeuroImage 47 (3), 1092–1104.
Biswal, B., DeYoe, E.A., Hyde, J.S., 1996. Reduction of physiological fluctuations in fMRI using digital filters. Magn. Reson. Med. 35 (1), 107–113.
Biswal, B., Yetkin, F.Z., Haughton, V.M., Hyde, J.S., 1995. Functional connectivity in the motor cortex of resting human brain using echo-planar MRI. Magn. Reson. Med. 34 (4), 537–541.
Bodurka, J., Ye, F., Petridou, N., Murphy, K., Bandettini, P.A., 2007. Mapping the MRI voxel volume in which thermal noise matches physiological noise-implications for fMRI. NeuroImage 34 (2), 542–549.
Bright, M.G., Murphy, K., 2013. Removing motion and physiological artifacts from intrinsic BOLD fluctuations using short echo data. NeuroImage 64, 526–537.
Bright, M.G., Murphy, K., 2015. Is fMRI “noise” really noise? Resting state nuisance regressors remove variance with network structure. NeuroImage 114, 158–169.
Brookes, M.J., Woolrich, M., Luckhoo, H., Price, D., Hale, J.R., Stephenson, M.C., Barnes, G.R., Smith, S.M., Morris, P.G., 2011. Investigating the electrophysiological basis of resting state networks using magnetoencephalography. Proc. Natl. Acad. Sci. USA 108 (40), 16783–16788.
Brooks, J.C.W., Faull, O.K., Pattinson, K.T.S., Jenkinson, M., 2013. Physiological noise in brainstem FMRI. Front. Hum. Neurosci. 7, 623.
Brosch, J.R., Talavage, T.M., Ulmer, J.L., Nyenhuis, J.A., 2002. Simulation of human respiration in fMRI with a mechanical model. IEEE Trans. Bio-Med. Eng. 49 (7), 700–707.
Buur, P.F., Poser, B.A., Norris, D.G., 2009. A dual echo approach to removing motion artefacts in fMRI time series. NMR Biomed. 22 (5), 551–560.

Buxton, R.B., Uludağ, K., Dubowitz, D.J., Liu, T.T., 2004. Modeling the hemodynamic response to brain activation. NeuroImage 23 (Suppl. 1), S220–S233.
Chang, C., Glover, G.H., 2009. Effects of model-based physiological noise correction on default mode network anti-correlations and correlations. NeuroImage 47 (4), 1448–1459.
Chang, C., Cunningham, J.P., Glover, G.H., 2009. Influence of heart rate on the BOLD signal: the cardiac response function. NeuroImage 44 (3), 857–869.
Chang, C., Raven, E.P., Duyn, J.H., 2016. Brain-heart interactions: challenges and opportunities with functional magnetic resonance imaging at ultra-high field. Philos. Trans. Ser. A Math. Phys. Eng. Sci. 374, 2067.
Chuang, K.H., Chen, J.H., 2001. IMPACT: image-based physiological artifacts estimation and correction technique for functional MRI. Magn. Reson. Med. 46 (2), 344–353.
Churchill, N.W., Spring, R., Afshin-Pour, B., Dong, F., Strother, S.C., 2015. An automated, adaptive framework for optimizing preprocessing pipelines in task-based functional MRI. PLoS One 10 (7), e0131520.
Cordes, D., Haughton, V.M., Arfanakis, K., Carew, J.D., Turski, P.A., Moritz, C.H., Quigley, M.A., Meyerand, M.E., 2001. Frequencies contributing to functional connectivity in the cerebral cortex in "resting-state" data. AJNR Am. J. Neuroradiol. 22 (7), 1326–1333.
Cox, R.W., 1996. AFNI: software for analysis and visualization of functional magnetic resonance neuroimages. Comput. Biomed. Res. Int. J. 29 (3), 162–173.
Curtis, A.T., Menon, R.S., 2014. Highcor: a novel data-driven regressor identification method for BOLD fMRI. NeuroImage 98, 184–194.
Dagli, M.S., Ingeholm, J.E., Haxby, J.V., 1999. Localization of cardiac-induced signal change in fMRI. NeuroImage 9 (4), 407–415.
De Martino, F., Gentile, F., Esposito, F., Balsi, M., Di Salle, F., Goebel, R., Formisano, E., 2007. Classification of fMRI independent components using IC-fingerprints and support vector machine classifiers. NeuroImage 34 (1), 177–194.
Edelstein, W.A., Glover, G.H., Hardy, C.J., Redington, R.W., 1986. The intrinsic signal-to-noise ratio in NMR imaging. Magn. Reson. Med. 3 (4), 604–618.
Evans, J.W., Kundu, P., Horovitz, S.G., Bandettini, P.A., 2015. Separating slow BOLD from non-BOLD baseline drifts using multi-echo fMRI. NeuroImage 105, 189–197.
Falahpour, M., Refai, H., Bodurka, J., 2013. Subject specific BOLD fMRI respiratory and cardiac response functions obtained from global signal. NeuroImage 72, 252–264.
Foerster, B.U., Tomasi, D., Caparelli, E.C., 2005. Magnetic field shift due to mechanical vibration in functional magnetic resonance imaging. Magn. Reson. Med.: Off. J. Soc. Magn. Reson. Med./Soc. Magn. Reson. Med., Nov., vol. 54(5), pp. 1261–1267.
Fox, M.D., Raichle, M.E., 2007. Spontaneous fluctuations in brain activity observed with functional magnetic resonance imaging. Nat. Rev. Neurosci. 8 (9), 700–711.
Fox, M.D., Snyder, A.Z., Vincent, J.L., Raichle, M.E., 2007. Intrinsic fluctuations within cortical systems account for intertrial variability in human behavior. Neuron 56 (1), 171–184.
Fox, M.D., Zhang, D., Snyder, A.Z., Raichle, M.E., 2009. The global signal and observed anticorrelated resting state brain networks. J. Neurophysiol. 101 (6), 3270–3283.
Frank, L.R., Buxton, R.B., Wong, E.C., 2001. Estimation of respiration-induced noise fluctuations from undersampled multislice fMRI data. Magn. Reson. Med. 45 (4), 635–644.
Friedman, L., Glover, G.H., 2006. Report on a multicenter fMRI quality assurance protocol. J. Magn. Reson. Imag.: JMRI 23 (6), 827–839.
Friston, K.J., Frith, C.D., Frackowiak, R.S., Turner, R., 1995. Characterizing dynamic brain responses with fMRI: a multivariate approach. NeuroImage 2 (2), 166–172.
Friston, K.J., Williams, S., Howard, R., Frackowiak, R.S., Turner, R., 1996. Movement-related effects in fMRI time-series. Magn. Reson. Med. 35 (3), 346–355.
Gao, J.-H., Liu, H.-L., 2012. Inflow effects on functional MRI. NeuroImage 62 (2), 1035–1039.
Gawryluk, J.R., Mazerolle, E.L., D'Arcy, R.C.N., 2014. Does functional MRI detect activation in white matter? A review of emerging evidence, issues, and future directions. Front. Neurosci. 8, 239.
Glover, G.H., Li, T.Q., Ress, D., 2000. Image-based method for retrospective correction of physiological motion effects in fMRI: RETROICOR. Magn. Reson. Med. 44 (1), 162–167.
Glover, G.H., Lemieux, S.K., Drangova, M., Pauly, J.M., 1996. Decomposition of inflow and blood oxygen level-dependent (BOLD) effects with dual-echo spiral gradient-recalled echo (GRE) fMRI. Magn. Reson. Med. 35 (3), 299–308.
Glover, G.H., Mueller, B.A., Turner, J.A., van Erp, T.G.M., Liu, T.T., Greve, D.N., Voyvodic, J.T., Rasmussen, J., Brown, G.G., Keator, D.B., Calhoun, V.D., Lee, H.J., Ford, J.M., Mathalon, D.H., Diaz, M., O'Leary, D.S., Gadde, S., Preda, A., Lim, K.O., Wible, C.G., Stern, H.S., Belger, A., McCarthy, G., Ozyurt, B., Potkin, S.G., 2012. Function biomedical informatics research network recommendations for prospective multicenter functional MRI studies. J. Magn. Reson. Imag.: JMRI 36 (1), 39–54.
Goldman, R.I., Stern, J.M., Engel, J., Cohen, M.S., 2002. Simultaneous EEG and fMRI of the alpha rhythm. Neuroreport 13 (18), 2487–2492.
Gonzalez-Castillo, J., Roopchansingh, V., Bandettini, P.A., Bodurka, J., 2011. Physiological noise effects on the flip angle selection in BOLD fMRI. NeuroImage 54 (4), 2764–2778.
Greicius, M.D., Srivastava, G., Reiss, A.L., Menon, V., 2004. Default-mode network activity distinguishes Alzheimer's disease from healthy aging: evidence from functional MRI. Proc. Natl. Acad. Sci. USA 101 (13), 4637–4642.
Greve, D.N., Brown, G.G., Mueller, B.A., Glover, G., Liu, T.T., 2013. A survey of the sources of noise in fMRI. Psychometrika 78 (3), 396–416.
Greve, D.N., Mueller, B.A., Liu, T., Turner, J.A., Voyvodic, J., Yetter, E., Diaz, M., McCarthy, G., Wallace, S., Roach, B.J., Ford, J.M., Mathalon, D.H., Calhoun, V.D., Wible, C.G., Brown, G.G., Potkin, S.G., Glover, G., 2011. A novel method for quantifying scanner instability in fMRI. Magn. Reson. Med. 65 (4), 1053–1061.
Hahamy, A., Calhoun, V., Pearlson, G., Harel, M., Stern, N., Attar, F., Malach, R., Salomon, R., 2014. Save the global: global signal connectivity as a tool for studying clinical populations with functional magnetic resonance imaging. Brain Connect. 4 (4), 395–403.
Hajnal, J.V., Myers, R., Oatridge, A., Schwieso, J.E., Young, I.R., Bydder, G.M., 1994. Artifacts due to stimulus correlated motion in functional imaging of the brain. Magn. Reson. Med. 31 (3), 283–291.
He, H., Liu, T.T., 2012. A geometric view of global signal confounds in resting-state functional MRI. NeuroImage 59 (3), 2339–2348.
Hu, X., Le, T.H., Parrish, T., Erhard, P., 1995. Retrospective estimation and correction of physiological fluctuation in functional MRI. Magn. Reson. Med. 34 (2), 201–212.
Iacovella, V., Hasson, U., 2011. The relationship between BOLD signal and autonomic nervous system functions: implications for processing of "physiological noise". Magn. Reson. Imag. 29 (10), 1338–1345.
Jiang, A., Kennedy, D.N., Baker, J.R., Weisskoff, R.M., Tootell, R.B.H., Woods, R.P., Benson, R.R., Kwong, K.K., Brady, T.J., Rosen, B.R., Belliveau, J.W., 1995. Motion detection and correction in functional MR imaging. Hum. Brain Mapp. 3, 224–235.
Jo, H.J., Saad, Z.S., Simmons, W.K., Milbury, L.A., Cox, R.W., 2010. Mapping sources of correlation in resting state FMRI, with artifact detection and removal. NeuroImage 52 (2), 571–582.
Johnstone, T., Ores Walsh, K.S., Greischar, L.L., Alexander, A.L., Fox, A.S., Davidson, R. J., Oakes, T.R., 2006. Motion correction and the use of motion covariates in multiple-subject fMRI analysis. Hum. Brain Mapp. 27 (10), 779–788.
Josephs, O., Howesman, A.M., Friston, K.J., Turner, R., 2007. Physiological noise modelling for multi-slice EPI fMRI using SPM. In: 5th ISMRM Scientific Meeting. Vancouver, Mar. p. 1682.
Kelly, R.E., Alexopoulos, G.S., Wang, Z., Gunning, F.M., Murphy, C.F., Morimoto, S.S., Kanellopoulos, D., Jia, Z., Lim, K.O., Hoptman, M.J., 2010. Visual inspection of independent components: defining a procedure for artifact removal from fMRI data. J. Neurosci. Methods 189 (2), 233–245.
Krüger, G., Glover, G.H., 2001. Physiological noise in oxygenation-sensitive magnetic resonance imaging. Magn. Reson. Med. 46 (4), 631–637.
Kundu, P., Inati, S.J., Evans, J.W., Luh, W.M., Bandettini, P.A., 2012. Differentiating BOLD and non-BOLD signals in fMRI time series using multi-echo EPI. NeuroImage 60 (3), 1759–1770.
Le, T.H., Hu, X., 1996. Retrospective estimation and correction of physiological artifacts in fMRI by direct extraction of physiological activity from MR data. Magn. Reson. Med. 35, 290–298.
Liu, T.T., Wong, E.C., 2005. A signal processing model for arterial spin labeling functional MRI. NeuroImage 24 (1), 207–215.
Liu, T.T., Frank, L.R., Wong, E.C., Buxton, R.B., 2001. Detection power, estimation efficiency, and predictability in event-related fMRI. NeuroImage 13 (4), 759–773.
Liu, T.T., Glover, G.H., Mueller, B.A., Greve, D.N., Rasmussen, J., Voyvodic, J.T., Turner, J.A., van Erp, T.G.M., Mathalon, D.H., Andersen, K., Kun, L., Brown, G.G., Keator, D.B., Calhoun, V.D., Lee, H.J., Ford, J.M., Diaz, M., O'Leary, D.S., Gadde, S., Preda, A., Lim, K.O., Wible, C.G., Stern, H.S., Belger, A., McCarthy, G., Ozyurt, B., Potkin, S.G., 2015. Quality Assurance in Functional MRI. In: Ugurbil, K., Berliner, L., Uludag, K. (Eds.), fMRI: From Nuclear Spins to Brain Function. Springer Verlag, Ch. 10, pp. 245–270.
Lund, T.E., Madsen, K.H., Sidaros, K., Luo, W.-L., Nichols, T.E., 2006. Non-white noise in fMRI: does modelling have an impact? NeuroImage 29 (1), 54–66.
Macey, P.M., Macey, K.E., Kumar, R., Harper, R.M., 2004. A method for removal of global effects from fMRI time series. NeuroImage 22 (1), 360–366.
Maclaren, J., Aksoy, M., Bammer, R., 2015. Contact-free physiological monitoring using a markerless optical system. Magn. Reson. Med. 74 (2), 571–577.
Maclaren, J., Herbst, M., Speck, O., Zaitsev, M., 2013. Prospective motion correction in brain imaging: a review. Magn. Reson. Med. 69 (3), 621–636.
Mayhew, S.D., Mullinger, K.J., Ostwald, D., Porcaro, C., Bowtell, R., Bagshaw, A.P., Francis, S.T., 2016. Global signal modulation of single-trial fMRI response variability: effect on positive vs negative BOLD response relationship. NeuroImage 133, 62–74.
McKeown, M.J., Makeig, S., Brown, G.G., Jung, T.-P., Kindermann, S.S., Bell, A.J., Sejnowski, T.J., 1998. Analysis of fMRI data by blind separation into independent spatial components. Hum. Brain Mapp. 6 (3), 160–188.
Menon, R.S., Ogawa, S., Tank, D.W., Ugurbil, K., 1993. 4 Tesla gradient recalled echo characteristics of photic stimulation-induced signal changes in the human primary visual cortex. Magn. Reson. Med.: Off. J. Soc. Magn. Reson. Med./Soc. Magn. Reson. Med., Sep., vol. 30(3), pp. 380–386.
Murphy, K., Birn, R.M., Bandettini, P.A., 2013. Resting-state fMRI confounds and cleanup. NeuroImage 80, 349–359.
Murphy, K., Birn, R.M., Handwerker, D.A., Jones, T.B., Bandettini, P.A., 2009. The impact of global signal regression on resting state correlations: are anti-correlated networks introduced? NeuroImage 44 (3), 893–905.
Muschelli, J., Nebel, M.B., Caffo, B.S., Barber, A.D., Pekar, J.J., Mostofsky, S.H., 2014. Reduction of motion-related artifacts in resting state fMRI using aCompCor. NeuroImage 96, 22–35.
Nishimura D.G., Principles of Magnetic Resonance Imaging, 2010 Stanford University, http://www.lulu.com/shop/dwight-nishimura/principles-of-magnetic-resonance-imaging/paperback/product-22829760.html.

Olafsson, V., Kundu, P., Wong, E.C., Bandettini, P.A., Liu, T.T., 2015. Enhanced identification of BOLD-like components with multi-echo simultaneous multi-slice (MESMS) fMRI and multi-echo ICA. NeuroImage 112, 43–51.
Ooi, M.B., Muraskin, J., Zou, X., Thomas, W.J., Krueger, S., Aksoy, M., Bammer, R., Brown, T.R., 2013. Combined prospective and retrospective correction to reduce motion-induced image misalignment and geometric distortions in EPI. Magn. Reson. Med. 69 (3), 803–811.
Parrish, T.B., Gitelman, D.R., LaBar, K.S., Mesulam, M.M., 2000. Impact of signal-to-noise on functional MRI. Magn. Reson. Med. 44 (6), 925–932.
Patriat, R., Molloy, E.K., Birn, R.M., 2015. Using edge voxel information to improve motion regression for rs-fMRI connectivity studies. Brain Connect. 5 (9), 582–595.
Peng, T., Niazy, R., Payne, S.J., Wise, R.G., 2013. The effects of respiratory CO_2 fluctuations in the resting-state BOLD signal differ between eyes open and eyes closed. Magn. Reson. Imag. 31 (3), 336–345.
Perlbarg, V., Bellec, P., Anton, J.-L., Pélégrini-Issac, M., Doyon, J., Benali, H., 2007. CORSICA: correction of structured noise in fMRI by automatic identification of ICA components. Magn. Reson. Imag. 25 (1), 35–46.
Pfeuffer, J., Van De Moortele, P.-F., Ugurbil, K., Hu, X., Glover, G.H., 2002. Correction of physiologically induced global off-resonance effects in dynamic echo-planar and spiral functional imaging. Magn. Reson. Med. 47 (2), 344–353.
Power, J.D., Schlaggar, B.L., Petersen, S.E., 2015. Recent progress and outstanding issues in motion correction in resting state fMRI. NeuroImage 105, 536–551.
Power, J.D., Barnes, K.A., Snyder, A.Z., Schlaggar, B.L., Petersen, S.E., 2012. Spurious but systematic correlations in functional connectivity MRI networks arise from subject motion. NeuroImage 59 (3), 2142–2154.
Pruim, R.H.R., Mennes, M., Buitelaar, J.K., Beckmann, C.F., 2015a. Evaluation of ICA-AROMA and alternative strategies for motion artifact removal in resting state fMRI. NeuroImage 112, 278–287.
Pruim, R.H.R., Mennes, M., van Rooij, D., Llera, A., Buitelaar, J.K., Beckmann, C.F., 2015b. ICA-AROMA: a robust ICA-based strategy for removing motion artifacts from fMRI data. NeuroImage 112, 267–277.
Purdon, P.L., Weisskoff, R.M., 1998. Effect of temporal autocorrelation due to physiological noise and stimulus paradigm on voxel-level false-positive rates in fMRI. Hum. Brain Mapp. 6 (4), 239–249.
Raj, D., Anderson, A.W., Gore, J.C., 2001. Respiratory effects in human functional magnetic resonance imaging due to bulk susceptibility changes. Phys. Med. Biol. 46 (12), 3331–3340.
Restom, K., Behzadi, Y., Liu, T.T., 2006. Physiological noise reduction for arterial spin labeling functional MRI. NeuroImage 31 (3), 1104–1115.
Rummel, C., Verma, R.K., Schöpf, V., Abela, E., Hauf, M., Berruecos, J.F.Z., Wiest, R., 2013. Time course based artifact identification for independent components of resting-state FMRI. Front. Hum. Neurosci. 7, 214.
Salimi-Khorshidi, G., Douaud, G., Beckmann, C.F., Glasser, M.F., Griffanti, L., Smith, S. M., 2014. Automatic denoising of functional MRI data: combining independent component analysis and hierarchical fusion of classifiers. NeuroImage 90, 449–468.
Särkkä, S., Solin, A., Nummenmaa, A., Vehtari, A., Auranen, T., Vanni, S., Lin, F.-H., 2012. Dynamic retrospective filtering of physiological noise in BOLD fMRI: DRIFTER. NeuroImage 60 (2), 1517–1527.
Satterthwaite, T.D., Wolf, D.H., Loughead, J., Ruparel, K., Elliott, M.A., Hakonarson, H., Gur, R.C., Gur, R.E., 2012. Impact of in-scanner head motion on multiple measures of functional connectivity: relevance for studies of neurodevelopment in youth. NeuroImage 60 (1), 623–632.
Shmueli, K., Van Gelderen, P., De Zwart, J.A., Horovitz, S.G., Fukunaga, M., Jansma, J. M., Duyn, J.H., 2007. Low-frequency fluctuations in the cardiac rate as a source of variance in the resting-state fMRI BOLD signal. NeuroImage 38 (2), 306–320.
Siegel, J.S., Power, J.D., Dubis, J.W., Vogel, A.C., Church, J.A., Schlaggar, B.L., Petersen, S.E., 2014. Statistical improvements in functional magnetic resonance imaging analyses produced by censoring high-motion data points. Hum. Brain Mapp. 35 (5), 1981–1996.
Smith, A.M., Lewis, B.K., Ruttimann, U.E., Ye, F.Q., Sinnwell, T.M., Yang, Y., Duyn, J.H., Frank, J.A., 1999. Investigation of low frequency drift in fMRI signal. NeuroImage 9 (5), 526–533.
Smith, S.M., Beckmann, C.F., Andersson, J., Auerbach, E.J., Bijsterbosch, J., Douaud, G., Duff, E., Feinberg, D.A., Griffanti, L., Harms, M.P., Kelly, M., Laumann, T., Miller, K. L., Moeller, S., Petersen, S., Power, J., Salimi-Khorshidi, G., Snyder, A.Z., Vu, A.T., Woolrich, M.W., Xu, J., Yacoub, E., Ugurbil, K., Van Essen, D.C., Glasser, M.F., 2013. WU-minn HCP consortium, resting-state fMRI in the human connectome project. NeuroImage 80, 144–168.
Sochat, V., Supekar, K., Bustillo, J., Calhoun, V., Turner, J.A., Rubin, D.L., 2014. A robust classifier to distinguish noise from fMRI independent components. PLoS One 9 (4), e95493.
Speck, O., Hennig, J., 1998. Functional imaging by I0- and T2*-parameter mapping using multi-image EPI. Magn. Reson. Med. 40 (2), 243–248.
Tagliazucchi, E., von Wegner, F., Morzelewski, A., Brodbeck, V., Laufs, H., 2012. Dynamic BOLD functional connectivity in humans and its electrophysiological correlates. Front. Hum. Neurosci. 6, 339.
Thomas, C.G., Harshman, R.A., Menon, R.S., 2002. Noise reduction in BOLD-based fMRI using component analysis. NeuroImage 17 (3), 1521–1537.
Tohka, J., Foerde, K., Aron, A.R., Tom, S.M., Toga, A.W., Poldrack, R.A., 2008. Automatic independent component labeling for artifact removal in fMRI. NeuroImage 39 (3), 1227–1245.
Tong, Y., Frederick, B.D., 2014. Studying the spatial distribution of physiological effects on BOLD signals using ultrafast fMRI. Front. Hum. Neurosci. 8, 196.
Tong, Y., Hocke, L.M., Frederick, B.D., 2014. Short repetition time multiband echo-planar imaging with simultaneous pulse recording allows dynamic imaging of the cardiac pulsation signal. Magn. Reson. Med. 72 (5), 1268–1276.
Tong, Y., Hocke, L.M., Fan, X., Janes, A.C., Frederick, B.D., 2015. Can apparent resting state connectivity arise from systemic fluctuations? Front. Hum. Neurosci. 9, 285.
Triantafyllou, C., Hoge, R.D., Krueger, G., Wiggins, C.J., Potthast, A., Wiggins, G.C., Wald, L.L., 2005. Comparison of physiological noise at 1.5 T, 3 T and 7 T and optimization of fMRI acquisition parameters. NeuroImage 26 (1), 243–250.
Van Dijk, K.R.A., Sabuncu, M.R., Buckner, R.L., 2012. The influence of head motion on intrinsic functional connectivity MRI. NeuroImage 59 (1), 431–438.
Wang, J., Aguirre, G.K., Kimberg, D.Y., Detre, J.A., 2003a. Empirical analyses of null-hypothesis perfusion FMRI data at 1.5 and 4 T. NeuroImage 19 (4), 1449–1462.
Wang, J., Aguirre, G.K., Kimberg, D.Y., Roc, A.C., Li, L., Detre, J.A., 2003b. Arterial spin labeling perfusion fMRI with very low task frequency. Magn. Reson. Med. 49 (5), 796–802.
Weisskoff, R.M., 1996. Simple measurement of scanner stability for functional NMR imaging of activation in the brain. Magn. Reson. Med. 36 (4), 643–645.
Weisskoff, R.M., Baker, J., Belliveau, J.W., Davis, T.L., Kwong, K.K., Cohen, M.S., Rosen, B.R., 1993. Power Spectrum Analysis of Functionally-Weighted MR Data: What's in the Noise? In: 12th Annual Scientific Meeting of the ISMRM. Apr. p. 7.
Wen, H., Liu, Z., 2016. Broadband electrophysiological dynamics contribute to global resting-state fMRI signal. J. Neurosci. 36 (22), 6030–6040.
Windischberger, C., Langenberger, H., Sycha, T., Tschernko, E.M., Fuchsjäger-Mayerl, G., Schmetterer, L., Moser, E., 2002. On the origin of respiratory artifacts in BOLD-EPI of the human brain. Magn. Reson. Imag. 20 (8), 575–582.
Wise, R.G., Ide, K., Poulin, M.J., Tracey, I., 2004. Resting fluctuations in arterial carbon dioxide induce significant low frequency variations in BOLD signal. NeuroImage 21 (4), 1652–1664.
Wong, C.-K., Zotev, V., Misaki, M., Phillips, R., Luo, Q., Bodurka, J., 2016. Automatic EEG-assisted retrospective motion correction for fMRI (aE-REMCOR). NeuroImage 129, 133–147.
Wong, C.W., Olafsson, V., Tal, O., Liu, T.T., 2013. The amplitude of the resting-state fMRI global signal is related to EEG vigilance measures. NeuroImage 83, 983–990.
Wong, C.W., Olafsson, V., Plank, M., Snider, J., Halgren, E., Poizner, H., Liu, T.T., 2014. Resting-state fMRI activity predicts unsupervised learning and memory in an immersive virtual reality environment. PLoS One 9 (10), e109622.
Yan, L., Zhuo, Y., Ye, Y., Xie, S.X., An, J., Aguirre, G.K., Wang, J., 2009. Physiological origin of low-frequency drift in blood oxygen level dependent (BOLD) functional magnetic resonance imaging (fMRI). Magn. Reson. Med. 61 (4), 819–827.
Yancey, S.E., Rotenberg, D.J., Tam, F., Chiew, M., Ranieri, S., Biswas, L., Anderson, K.J. T., Baker, S.N., Wright, G.A., Graham, S.J., 2011. Spin-history artifact during functional MRI: potential for adaptive correction. Med. Phys. 38 (8), 4634–4646.
Yang, G.J., Murray, J.D., Repovs, G., Cole, M.W., Savic, A., Glasser, M.F., Pittenger, C., Krystal, J.H., Wang, X.-J., Pearlson, G.D., Glahn, D.C., Anticevic, A., 2014. Altered global brain signal in schizophrenia. Proc. Natl. Acad. Sci. USA 111 (20), 7438–7443.
Yuan, H., Zotev, V., Phillips, R., Bodurka, J., 2013. Correlated slow fluctuations in respiration, EEG, and BOLD fMRI. NeuroImage 79, 81–93.
Yuan, H., Ding, L., Zhu, M., Zotev, V., Phillips, R., Bodurka, J., 2016. Reconstructing large-scale brain resting-state networks from high-resolution EEG: spatial and temporal comparisons with fMRI. Brain Connect. 6 (2), 122–135.
Zarahn, E., Aguirre, G.K., D'esposito, M., 1997. Empirical analyses of BOLD fMRI statistics. I. spatially unsmoothed data collected under null-hypothesis conditions. NeuroImage 5 (3), 179–197.
Zeng, L.-L., Wang, D., Fox, M.D., Sabuncu, M., Hu, D., Ge, M., Buckner, R.L., Liu, H., 2014. Neurobiological basis of head motion in brain imaging. Proc. Natl. Acad. Sci. USA 111 (16), 6058–6062.
Zhao, X., Bodurka, J., Jesmanowicz, A., Li, S.J., 2000. B(0)-fluctuation-induced temporal variation in EPI image series due to the disturbance of steady-state free precession. Magn. Reson. Med.: Off. J. Soc. Magn. Reson. Med./Soc. Magn. Reson. Med., Nov. , vol. 44(5), pp. 758–765.
Zou, Q., Ross, T.J., Gu, H., Geng, X., Zuo, X.-N., Hong, L.E., Gao, J.-H., Stein, E.A., Zang, Y.-F., Yang, Y., 2012. Intrinsic resting-state activity predicts working memory brain activation and behavioral performance. Hum. Brain Mapp. 34 (12), 3204–3215.